Role of substrate and TiO_2 content in TiO_2:Ta_2O_5 coatings for gravitational wave detectors

Ofelia Durante, Veronica Granata, Michele Magnozzi, Alex Amato, Christophe Michel, Laurent Pinard, Massimo Granata, Maurizio Canepa, Giovanni Carapella, Francesco Chiadini, et al.

Role of substrate and TiO_2 content in TiO_2:Ta_2O_5 coatings for gravitational wave detectors

OPEN ACCESS
IOP Publishing
Classical and Quantum Gravity
Class. Quantum Grav. **41** (2024) 025005 (14pp) https://doi.org/10.1088/1361-6382/ad1613

Role of substrate and TiO_2 content in TiO_2:Ta_2O_5 coatings for gravitational wave detectors

Ofelia Durante[1,2,3], Veronica Granata[1,2,*], Michele Magnozzi[4,5], Alex Amato[6], Christophe Michel[7], Laurent Pinard[7], Massimo Granata[7], Maurizio Canepa[4], Giovanni Carapella[1,2,3], Francesco Chiadini[2,8], Roberta De Simone[2,8], Rosalba Fittipaldi[2,3], Vincenzo Fiumara[2,9], Vincenzo Pierro[2,10], Innocenzo M Pinto[2,11], Antonio Vecchione[3], Fabrizio Bobba[1,2,3] and Cinzia Di Giorgio[1,12]

[1] Department of Physics 'E.R. Caianiello', University of Salerno, Fisciano, Italy
[2] National Institute of Nuclear Physics (INFN), Sezione di Napoli Gruppo Collegato di Salerno, Napoli, Italy
[3] National Research Council- SuPerconducting and other INnovative materials and devices institute (CNR-SPIN), c/o University of Salerno, Fisciano, Italy
[4] OptMatLab, Dipartimento di Fisica, Università di Genova, via Dodecaneso 33, 16146 Genova, Italy
[5] Istituto Nazionale di Fisica Nucleare, Sezione di Genova, via Dodecaneso 33, 16146 Genova, Italy
[6] Université de Lyon, Université Claude Bernard Lyon 1, CNRS, Institut Lumière Matière, F-69622 Villeurbanne, France
[7] Laboratoire des Matériaux Avancés—IP2I, CNRS, Université de Lyon, Université Claude Bernard Lyon 1, Villeurbanne F-69622, France
[8] Department of Industrial Engineering, DIIN, University of Salerno, Fisciano, Italy
[9] School of Engineering, University of Basilicata, Potenza, Italy
[10] Department of Engineering, DING, University of Sannio, Benevento, Italy
[11] Department Electrical and Information Technology Engineering, University of Naples 'Federico II', Napoli, Italy
[12] National Research Council- Materials Foundry Institute (CNR-IOM), Trieste, Italy

E-mail: vgranata@unisa.it

[*] Author to whom any correspondence should be addressed.

Received 27 October 2023; revised 30 November 2023
Accepted for publication 15 December 2023
Published 27 December 2023

Abstract

Gravitational wave detectors (GWDs) are designed to detect the elusive signals produced by spacetime ripples, the GWs. The key to improving GWD sensitivity relies on the reduction of the thermal noise introduced by the mirrors. The high refractive index component of the high-reflectance mirrors installed in the current generation GWDs, such as Advanced LIGO and Advanced Virgo, is made of a mixture of $\sim$27% TiO_2 and $\sim$73% Ta_2O_5. Such a coating plays a fundamental role in the GWD performance. The 27:73 TiO_2:Ta_2O_5 ratio ensures high structural, optical, and mechanical performances, which allowed for the first ever detection of GWs, but might not be enough for new generation GWDs. Here, we investigate the potential of TiO_2:Ta_2O_5 coatings, in a wider range of Ti/(Ta + Ti) cation ratio. Our research spans over the morphological and structural coating characteristics, and their correlation with optical and mechanical properties. On one hand, we unveil the profound influence of substrate selection and TiO_2 content on the quality of coating morphology. On the other, we pinpoint the effect of TiO_2 content on the structural properties of the coating, as increasing TiO_2 content leads to lower temperature amorphous-to-crystalline transition, and we show that internal strain may arise due to the coexistence of TiO_2 and Ta_2O_5 crystalline phases. Finally, substrate choice, TiO_2 concentration, and crystallization characteristics emerge as pivotal factors in the pursuit of precision optics.

Supplementary material for this article is available online

Keywords: gravitational wave detectors, coatings, morphological characteristics, structural characteristics, optical properties, crystallization

1. Introduction

The Brownian thermal noise of the dielectric mirror coatings is currently one of the main limitations in the sensitivity of high-performance optical applications, such as gravitational wave detectors (GWDs). Such noise arises from fluctuations of the GWD's mirror surface, due to the random motion of particles, occurring inside both the optical coating and its substrate (SiO_2) [1, 2]. The fluctuation-dissipation theorem [3] sets the relation between the intensity of such fluctuations and the internal friction-driven mechanical losses: the higher the friction occurring at local defects or at the boundaries between different phases inside the material, the higher the mechanical losses, the higher the thermal noise level. The mechanical losses occurring in the optical coatings are usually several orders of magnitude larger than those of the substrate [4–6]. Therefore, a considerable research effort has been committed to the development of high-quality optical coatings [6], as well as new coating designs have been proposed [7, 8], to reduce the thermal noise.

To date, amorphous oxides are the key constituents of optical coatings. In particular, the coatings for GWDs are composed of alternating high- and low-refractive index amorphous

oxides, TiO_2:Ta_2O_5 and SiO_2, respectively, in a Bragg geometry, deposited at room temperature using ion beam sputtering (IBS) at the Laboratoire des Materiaux Avances [9]. A cation mixing ratio, defined in percentage as Ti/(Ta + Ti), of 27% is currently used. Such mixture ($\sim$73% Ta_2O_5, $\sim$27% TiO_2) is dictated by the ability of TiO_2 to reduce Ta_2O_5 mechanical losses [10, 11], thus reducing the overall thermal noise of the resulting coating [12].

Internal friction, responsible for mechanical losses, can originate from different kinds of defects of the amorphous structure. A routine approach to reduce the defects relies on post-deposition thermal annealing. Granata *et al* [6] have studied the coating loss angle in TiO_2:Ta_2O_5 ($\sim$27:73) before and after annealing at 500 °C, demonstrating that a clear improvement arises upon thermal treatment. On the contrary, a net worsening of the coating loss angle is measured in pure TiO_2, after annealing at the same temperature. Amato *et al* [13] have extensively studied the optical and mechanical properties of TiO_2:Ta_2O_5 coatings, by systematically varying the cation mixing ratio, before and after the standard annealing procedure. They found out that, while the mechanical losses are quite low over a broad range of Ti/(Ta + Ti) ratio, the Urbach energy function, a parameter measuring the structural disorder, has a clear minimum in correspondence of the annealed 20% TiO_2:Ta_2O_5, which justifies the enhanced performance of the used mixture over other cation ratios.

In the present paper, we complement the existing measurements by investigating the morphological and structural quality of TiO_2:Ta_2O_5 coatings, with variable cation mixing ratio. We use an approach based on atomic force microscopy (AFM), x-ray diffraction (XRD), and Raman spectroscopy (RS) to deepen into the morphological and structural characteristics of the optical coatings, in their as-deposited form as well as after annealing treatments. Additionally, we use spectroscopic ellipsometry (SE) to derive the coating's refractive index, and its dependence on TiO_2 content and thermal annealing. The comprehensive understanding of the correlation between morphology/structure and optical/mechanical properties is pivotal to full control of the deposited material, and its optimization, to develop high-performance optical applications.

2. Materials and methods

2.1. Coating samples

The TiO_2:Ta_2O_5 coatings, studied in this paper, consist of amorphous oxide mixtures of various cation ratios Ti/(Ta + Ti) deposited by IBS at the Laboratoire des Materiaux Avances, using a custom made coating machine, the so-called Grand Coater [14], developed to deposit the large high-reflective mirrors for GWDs. Multiple coatings were deposited at the same time, on different substrates, so that different investigations could be carried out on expectedly identical samples. We used silicon (Si) wafers and silica (SiO_2) disk. The Si wafers were single side polished to avoid backside reflections during optical investigations. The SiO_2 disk were made of Corning 7980 A and polished on both surfaces to a residual root mean square (RMS) roughness of 1 nm, which is about 5 times higher than that of GWDs' substrates [15]. Thin SiO_2 disk were also used, in the past, for mechanical measurements on twin samples, as reported elsewhere [6, 13]. Table 1 provides the details of the investigated coatings, including the nominal Ti/(Ta + Ti) concentration, the correspondent value measured by energy dispersive spectroscopy (EDS) (reported in supplementary material), and their substrate. The thickness varies between 350 and 850 nm. From the morphological and structural point of view, all coatings in the investigated thickness range can be considered in the bulk regime, thus they are unaffected by thickness variation (see supplementary material for morphology and [16] for structural properties).

Table 1. List of coatings fabricated by IBS at the Laboratoire des Materiaux Avances.

Sample	Ti/(Ta + Ti) (%) nominal	Ti/(Ta + Ti) from EDS (%)	Substrate
Ta_2O_5	0	7.1 ± 0.6	Si, SiO_2
TiO_2:Ta_2O_5 (25%)	25	16.1 ± 0.5	Si, SiO_2
TiO_2:Ta_2O_5 (50%)	50	38 ± 1	Si
TiO_2:Ta_2O_5 (75%)	75	—	SiO_2
TiO_2:Ta_2O_5 (80%)	80	83 ± 1	Si, SiO_2
TiO_2:Ta_2O_5 (90%)	90	—	SiO_2
TiO_2	100	96 ± 1	Si, SiO_2

2.2. Thermal annealing

All coatings have been studied in the as-deposited phase as well as after annealing at 500 °C, which is the standard post-fabrication annealing temperature for GWD coatings so far adopted. The coatings produced on SiO_2 were annealed at LMA, in the air, for 10 h, by using a ramp rate of 100 °C h^{-1}. The annealing of the coatings produced on Si were performed in the air, in a homemade furnace, by using a heating rate of 3 °C min^{-1}, a 12 h plateau at a fixed temperature (between 250 °C and 1000 °C), and a cooling rate of 1 °C min^{-1}. The structural results demonstrate no dependence on the annealing process adopted. The coatings deposited on Si substrate underwent annealing in a wider temperature range. This allowed us not only to pinpoint the morphological and structural status after the standard post-deposition annealing procedure, but also to have a full control on the effect of annealing temperature on the structural and morphological coatings properties. Each treatment was performed on a pristine fragment of the as-grown sample, to avoid any memory effect of multiple subsequent heating/cooling cycles.

2.3. Morphological characterization

2.3.1. Atomic force microscopy (AFM). AFM images have been acquired with a JPK Nanowizard III, equipped with Vortex electronics, in the standard tapping mode technique, using a Bruker SCM-PIT-V2 tip. The tapping, or intermittent contact, mode guarantees a safer tip-sample interaction, compared to contact mode, with a consequent longer preservation of the tip shape. The longer tip lifetime allows to take multiple measurements with the same probe, thus to build a statistic; the stability of the tip shape allows for a meaningful comparison between multiple images. All data were analyzed by using the WSxM 5.0 software by NanoTec, 2015.

2.4. Structural characterization

2.4.1. X-ray diffraction (XRD). The XRD patterns were acquired at room temperature by using a D2 phaser diffractometer from Bruker with a time/step of 0.2 s, a 2θ step of 0.02°, and a 2θ angle ranging from 20° to 75°.

2.4.2. Raman spectroscopy (RS). The RS was performed by means of an inVia™ Renishaw Raman microscope, in the backscattering geometry, equipped with a near infrared laser excitation source, with a wavelength of 785 nm. The Raman spectra were acquired with 50× of

magnification, 10 s of exposure time, 5%–10% of laser power, and up to 5 accumulations. The accumulation number was chosen, time by time, as the best trade-off between a good signal-to-noise ratio and a reasonable acquisition time. Multiple spots have been sampled across the sample surface and the Raman spectra reported below are representative of the average Raman response. It is worth noting that all samples exhibited a uniform Raman behavior, independently of the probed region. Where present, cosmic rays were removed by using a standard median filtering.

2.5. Optical characterization

2.5.1. Spectroscopic ellipsometry (SE). The SE measurements were performed in the center of each sample. The light beam used to obtain ellipsometry data had a diameter of approximately 2 mm and the spectral range varied from 620 nm to 2100 nm (1100 nm in the case of pure as-deposited Ta_2O_5 coating). Each SE measurement consists of spectra acquired at three angles of incidence (55°, 60°, 65°) to maximize the sensitivity of the dataset. The refractive index was obtained by fitting the experimental SE data with a Cauchy dispersion relation, which is a well-established approach to describe the optical properties of coatings in their transparency region. SE data for this work were acquired with a J. A. Woollam Co. Variable Angle Spectroscopic Ellipsometer (VASE); SE data were analyzed with the WVASE 3.718 software by J. A. Woollam Co.

3. Results and discussion

The complete characterization of the coatings for the mirrors of GWDs encompasses the study of many properties, such as optical, mechanical, morphological, and structural, each affecting the mirror performance, in terms of reflectivity and thermal noise. Each study requires a slightly different support. As described in [13], Si wafers are used during optical investigations, to avoid backside reflections, while SiO_2 disk are preferred for mechanical measurements. Here we complement the study presented in [13], by investigating the role of the substrate on the morphological and structural properties of TiO_2:Ta_2O_5 coatings. From the morphological point of view, we performed a comprehensive study based on AFM: figure 1 shows the AFM topographies, 10 μm $\times$ 10 μm in lateral size, of the as-deposited TiO_2:Ta_2O_5 coatings with different compositions, nominally 0%, 25%, 80%, and 100%. The top and bottom rows refer to coatings deposited on SiO_2 and Si substrates, respectively.

A clear difference in surface topography arises as a function of the substrate used: when the coatings are deposited on SiO_2 (top row) a linear material arrangement occurs, with a peak to valley surface roughness of 7 nm (figures 1(a)–(c)); when the substrate is made of Si (bottom row) the coating growth is isotropic with a lower peak to valley surface roughness of 2 nm (figures 1(e)–(g)). When the coating composition is 100% (pure TiO_2), the nanometric or sub-nanometric surface features are masked by the occurrence of pinhole-like defects (rescaled images are reported in supplementary material) [17]. The different surface topographies, resembling a linear arrangement in the SiO_2 templated case and an isotropic growth in the Si one, are dictated by the morphological quality of the substrate used. Figures 2(a) and (b) shows the AFM topography of bare SiO_2 and Si, respectively. As one can notice, the SiO_2 bare substrate is itself characterized by linear structures, possibly coming from the polishing procedure. In contrast, the surface of Si is notably flat and smooth. The RMS roughness is 0.8 for SiO_2 and 0.6 for Si. This difference in surface characteristics has a direct and significant impact on the

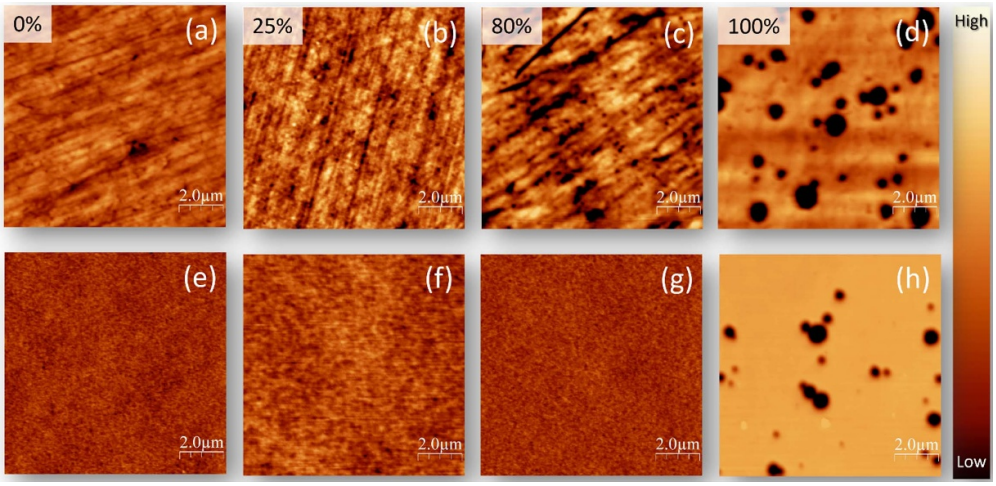

Figure 1. Tapping-mode AFM topographies on a large scan area (10 μm $\times$ 10 μm) of the as-deposited TiO_2:Ta_2O_5 on SiO_2: (a) 0%, (b) 25%, (c) 80%, (d) 100% and on Si (e) 0%, (f) 25%, (g) 80%, (h) 100%. The color scale ranges from: 0 to 7 nm in (a)–(c); 0–2 nm in (e), (g); and 0–60 nm in (d), (h).

overall roughness of the coatings deposited on top, even if they are quite thick (350–850 nm). Figure 2(c) shows the RMS roughness of the TiO_2:Ta_2O_5 coatings as a function of substrate and as a function of TiO_2 percentage.

At %TiO_2 varying between 0 and 80, the coatings deposited on SiO_2 exhibit a consistently higher RMS roughness, compared to the ones deposited on Si, reflecting their different surface topography, as templated by the substrate. The linear features observed on the SiO_2 substrate contribute to the increased roughness of the coatings grown on top, while the flat and smooth nature of the Si substrate surface leads to lower coating's roughness. This discrepancy in roughness values underscores the importance of substrate selection and its direct influence on the quality and surface characteristics of the deposited films, which is especially important for the mirrors used for high precision applications, such as GWDs. When %TiO_2 is higher than 80, the RMS roughness increases appreciably. This change is attributed to the formation of the pinhole defects, which impact significantly the surface quality [18]. As the RMS error bars are calculated over a statistical analysis of many sampled areas per each sample surface, the large variation (error bars) of RMS, measured at % $TiO_2 \geqslant 90\%$, reflects the randomicity of pinholes distribution on the sample surface, as well as their random depth (both parameters affect the RMSs). As the pinholes only appear at high %TiO_2, we studied the dependency of the pinhole density on %TiO_2. Figures 2(d)–(f) shows the evolution of surface morphology in TiO_2:Ta_2O_5 coatings, deposited on SiO_2, with %TiO_2 being 80, 90, and 100, respectively. As one can notice, at 80% few darker spots appear, which still do not have very well-defined circular shape. At 90%, the pinholes are well developed, and their typical circular shape can be observed, with a diameter <1 μm in average. Finally, at 100%, the pinholes have bigger size—the largest reaching $\sim$1.5 μm in diameter—and are more numerous. The inset of figure 2(c) shows the variation of the percentage area interested by pinholes as a function of %TiO_2. This percentage increases from 0.67 for 80% TiO_2 to 7.33 for 100% TiO_2. The correspondent analysis is reported in supplementary materials. It is worth noting that the occurrence of pinhole defects is independent of the substrate, as they appear both in the coatings deposited on SiO_2

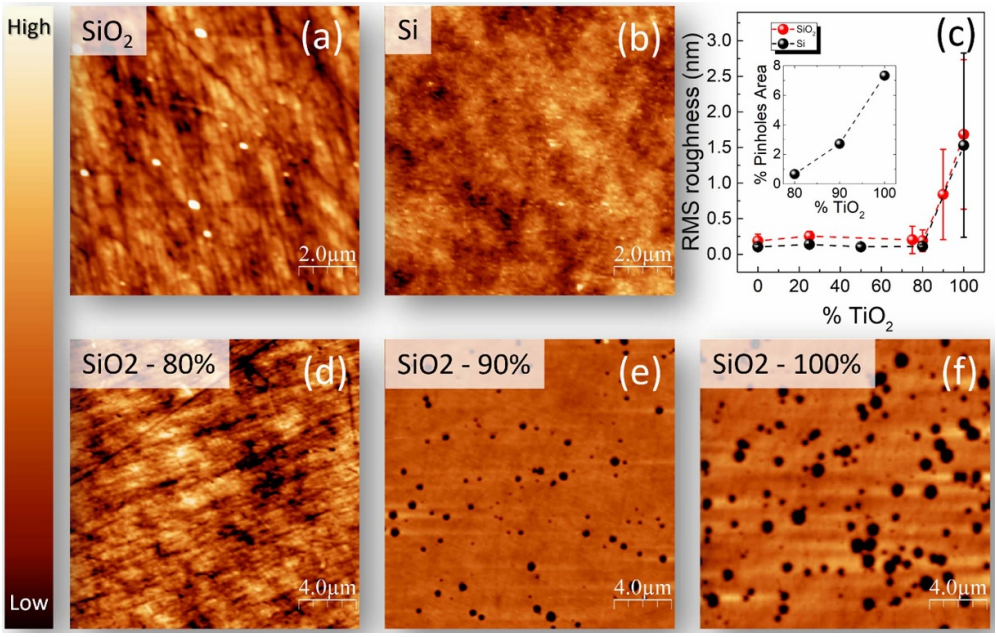

Figure 2. Tapping-mode AFM topographies on a large scan area (10 μm $\times$ 10 μm) of SiO_2 (a) and Si (b) substrate. (c) Main: RMS roughness vs %TiO_2 of the as-grown coatings. Inset: % pinhole area vs %TiO_2. Tapping-mode AFM topographies on a large scan area (20 μm $\times$ 20 μm) of as-grown TiO_2:Ta_2O_5 deposited on SiO_2: (d) 80%, (e) 90%, and (f) 100%. The color scale ranges from: 0 to 5 nm for (a), (b), and (d), and from 0 to 50 nm for (e) and (f).

and on Si, at high %TiO_2. It is known that the formation of these defects is highly dependent on deposition parameters, including sputtering power, substrate temperature, Ar pressure [18], which can affect different material in different manners. While the surface quality and roughness of pure Ta_2O_5 seems almost unaffected by the ion energy during IBS, up to more than 1 keV [19], an ion beam energy of 0.5 keV has already been shown to produce holes of few tens of nm in the surface of pure TiO_2 [20]. As the IBS energy used in producing the TiO_2:Ta_2O_5 coatings is 1 keV, and the pinholes only occur in high %TiO_2, with a density proportional to the % TiO_2, we believe that our observations reflect this property of TiO_2 to be more susceptible to defect generation by ion bombardment than Ta_2O_5.

Furthermore, we probed the crystallization status of as-deposited and annealed coatings by XRD and RS. Figure 3(a) shows the XRD spectra of the coatings deposited on SiO_2. All coatings were found amorphous in their as-deposited phase, independently on the %TiO_2. For simplicity of representation, we only show the spectrum of the as-grown 0% coating, in black. Here, a prominent bump is visible, between 10° and 40°, due to the amorphous SiO_2 substrate. Red spectra are the XRD patterns measured after annealing at 500 °C, as for the standard post-deposition process of coatings for GWD mirrors. No visible spectrum alternation occurs upon increasing the %TiO_2 from 0 to 75, i.e. the coatings remain amorphous. In contrast, the XRD spectra of the TiO_2:Ta_2O_5 80%, 90%, and 100% (pure TiO_2) exhibit the characteristic TiO_2 anatase reflections, specifically (101), (004), and (200). The blue curve is the reference spectrum of the TiO_2 anatase phase [21]. Thus, at %TiO_2 higher than 75 the coatings crystallize upon standard annealing at 500 °C.

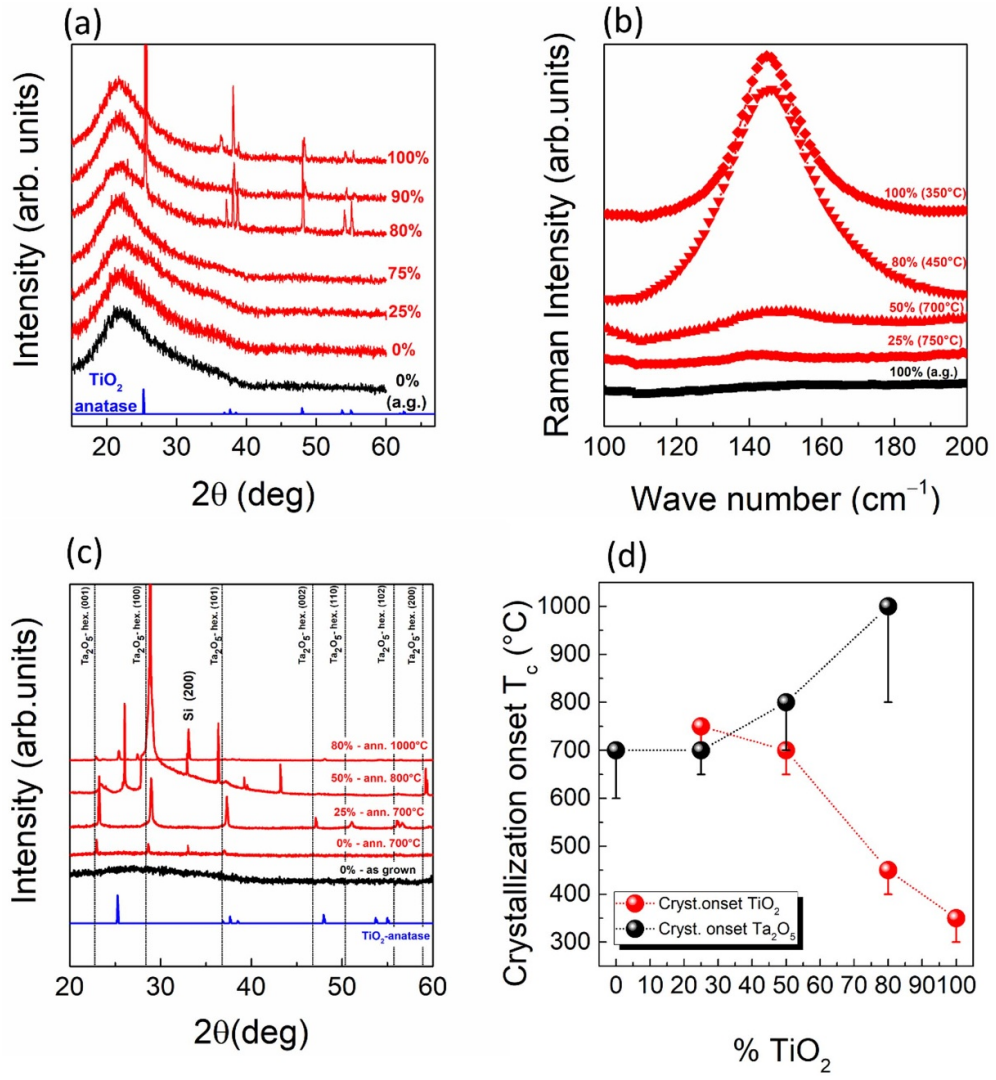

Figure 3. (a) XRD spectra of: 0% as-grown coating (black); 0%, 25%, 75%, 80%, 90%, and 100% 500 °C annealed coatings (red); reference TiO_2 anatase diffraction pattern [21] (blue). (b) RS spectra of: 100% as-grown coating (black); annealed coatings (red). (c) XRD spectra of: 0% as-grown coating (black); annealed coatings (red); hexagonal crystalline reflections of Ta_2O_5 [22] (black dashed lines). (d) T_c of the TiO_2 and Ta_2O_5, as a function of the TiO_2 concentration.

The behavior of the coatings deposited on Si (not shown here) matches that on SiO_2, with identical structural properties upon annealing at 500 °C. However, to have a comprehensive understanding of the crystallinity status of both TiO_2 and Ta_2O_5 components, inside the TiO_2:Ta_2O_5 mixture, we investigated a wider temperature range, going from 300 °C to 1000 °C, which is to date beyond the routinary process used for the coatings for GWDs. Knowing the crystallization onset temperature, T_c, of both TiO_2 and Ta_2O_5 vs %TiO_2 inside

the TiO_2: Ta_2O_5 mixture allows to build a phase diagram which predicts, given % TiO_2 and annealing temperature, the structural status of the final product.

We used RS to pinpoint the T_c of the TiO_2 crystalline phase inside the TiO_2:Ta_2O_5 mixture, as a function of %TiO_2. Figure 3(b) shows a series of Raman spectra acquired at the amorphous-to-crystalline transition temperature, focusing on the E_g Raman mode at ∼141.5–144 cm^{-1}, characteristic of the anatase TiO_2 crystalline phase (which is expected to appear at much lower temperature, compared to rutile). The Raman spectrum of the amorphous as-deposited 100% TiO_2, is shown in black. As one can see, the E_g peak develops at lower temperatures as the %TiO_2 increases, thus T_c decreases from 750 °C at 25% TiO_2 to 350 °C at 100% TiO_2. This result is summarized by the red scatters of figure 3(d). Furthermore, we used XRD to detect the amorphous-to-crystalline transition of the Ta_2O_5 component inside the TiO_2:Ta_2O_5 mixture.

Figure 3(c) shows, in black, the amorphous as-deposited 0% sample, where no reflections are observed. Crystalline peaks develop in the XRD pattern at increasing annealing temperature as the %TiO_2 is increased, going from 700 °C at 0% TiO_2, to 1000 °C at 80% TiO_2. These peaks are reflections from the hexagonal crystalline phase of Ta_2O_5 [22], as indicated by the black dashed vertical lines. As one can notice, these reflections appear at slightly shifted angles compared to the expected positions, probably due to the development of some internal strain. Indeed, the shift is especially evident at 25% and 50% TiO_2, at temperatures where also TiO_2 is in (or is close to) its crystalline state. The presence of a reciprocal imposed strain between TiO_2 and Ta_2O_5 crystalline phases reflects in the fact that also the TiO_2 peaks in the 50% and 80% spectrum are shifted with respect to the expected positions (anatase TiO_2 reference XRD spectrum is the blue curve). Based on the discussed findings, figure 3(d) shows the T_c of both the TiO_2 (red scatters) and Ta_2O_5 (black scatters) counterparts of the TiO_2:Ta_2O_5 coatings, as a function of TiO_2 concentration. The asymmetric error bar highlights the uncertainty in the determination of the exact T_c, due to the discrete steps used in the annealing process. As shown by figure 3(d), a distinct trend emerges: the lower the material concentration, the higher its T_c. This finding shed light on the intricate interplay between TiO_2 and Ta_2O_5 in these coatings. According to our crystallization results, the two materials remain quite segregated inside the overall coating, rather than mixing in a uniform phase.

We investigated the impact of heat treatments on the coating morphology by performing AFM measurements, after annealing at 500 °C. This morphological analysis complements the structural information obtained through XRD. In fact, as shown in figure 4, the 0% ((a), (e)) and 25% ((b), (f)) coatings preserve their as-deposited morphology, both on SiO_2 and Si substrates. This is consistent with the fact that these coatings stay amorphous upon annealing at 500 °C. On the contrary, when TiO_2 concentration is 80% or higher ((c), (d), (g), (h)), crystalline plates develop. Those features are attributed to the amorphous-to-crystalline structural transition [16, 23]. Pinholes are still observed at high %TiO_2, as the material crystallization is supposed to further densify the material, thus enhancing the appearance of hole-like defects.

Moreover, we employed RS to investigate the dynamics of crystallization. The complete set of measurements is reported in supplementary materials. Here, we show the characteristic Raman spectra acquired on the TiO_2:Ta_2O_5 coatings upon annealing at 750 °C (figure 5(a)). At this temperature all the studied coatings present a partially crystallized TiO_2 phase, as certified by the presence of the E_g Raman band, associated to the anatase phase, expected at ∼141.5–144 cm^{-1}. Notably, both the E_g peak position and its intensity vary from coating to coating. While the variation of the intensity depends on the volume of crystalline materials, and thus on the thickness of the coatings, the dependence of E_g peak position on %TiO_2, figure 5(b), gives us insight on the crystal structure. As shown in figure 5(b), when TiO_2 is

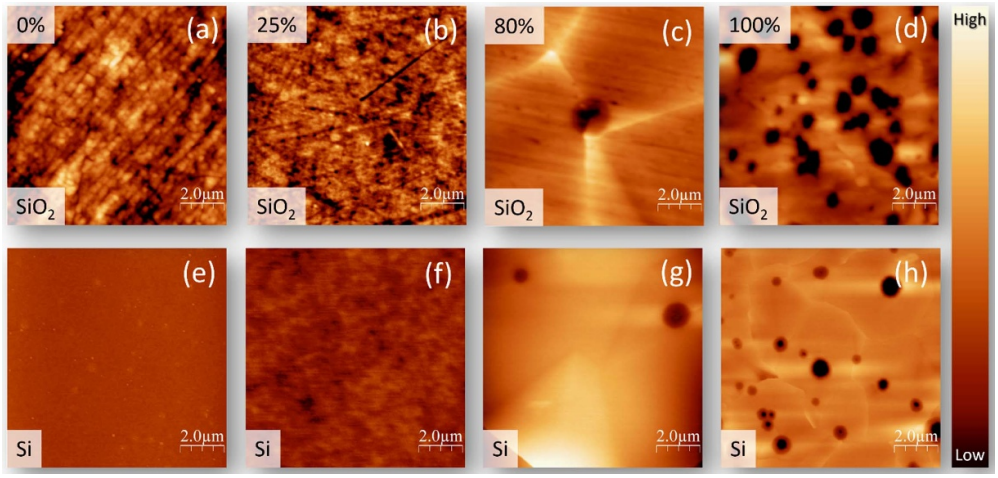

Figure 4. Tapping-mode AFM topographies on a large scan area (10 μm $\times$ 10 μm) of the TiO_2:Ta_2O_5 coatings annealed at 500 °C, and deposited on SiO_2 with (a) 0%, (b) 25%, (c) 80%, (d) 100% TiO_2 concentration; deposited on Si with (e) 0%, (f) 25%, (g) 80%, (h) 100% TiO_2 concentration. The color scale ranges from: 0 to 7 nm for (a)–(c); 0–2 nm for (e), (g); and 0–6 nm for (d), (h).

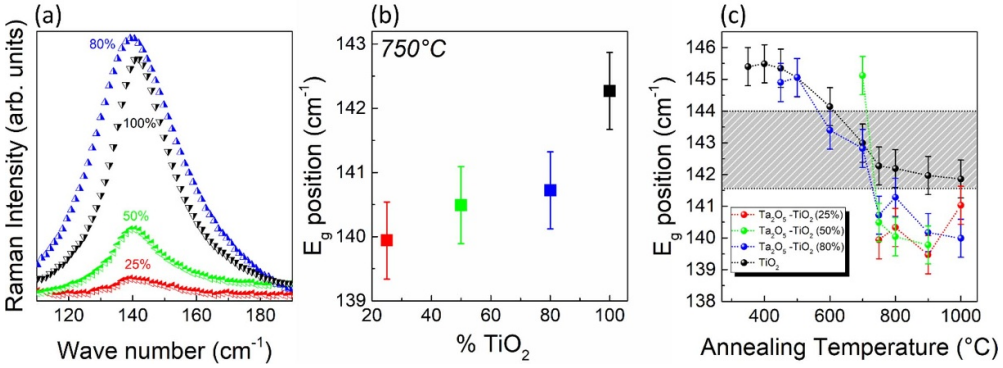

Figure 5. (a) Representative RS of TiO_2:Ta_2O_5 coatings: 25% (red), 50% (green), 80% (blue), and 100% (black) annealed at 750 °C, in the range 100–200 cm^{-1}. (b) E_g peak position as a function of TiO_2 concentration. (c) Raman shift vs annealing temperature. The gray region in (c) highlights the range where the E_g Raman mode is expected [21, 24].

in its pure phase (100%), the peak of the E_g band appears at its expected value. When the TiO_2 concentration is reduced, the E_g mode red-shifts with respect to the expected value. This observation suggests that, at low %TiO_2, the material is affected by tensile strain, as already found by XRD.

The temperature evolution of the E_g peak position, in a wider temperature range, is shown in figure 5(c). The exact peak position is extracted by removing the Si contribution and performing a Lorentzian fit of the as-treated data. The grey region indicates the reference wave number positions of the E_g mode, as reported in [21, 24]. Compared to these values, TiO_2:Ta_2O_5 (100%, 80% and 50%) (black, blue and green dots respectively), show a blue-shift in their

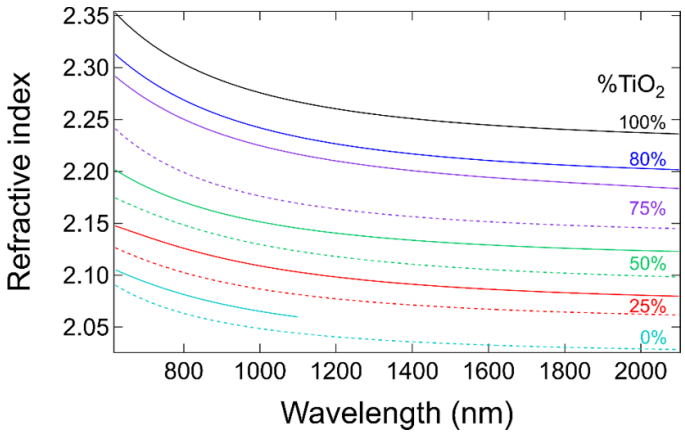

Figure 6. Refractive index vs. wavelength of TiO_2:Ta_2O_5 coatings as-deposited (solid line) and annealed at 500 °C (dashed line), in the near-infrared. The data for 0% TiO_2, are available only up to 1100 nm in this investigation; the refractive index of 80% and 100% TiO_2, annealed, are affected by post-annealing crystallization, and not reported here.

initial stage of crystallization. This phenomenon can be attributed to a crystallite size under the quantum-confinement condition, as usually occurs at the very beginning of crystallization [23]. A monotonic decrease of the E_g peak center, red-shifting as a function of the annealing temperature, is observed for all coatings. This behavior is due to the setting up of tensile strain, occurring because of Ta_2O_5 crystallization. In fact, the E_g peak of pure TiO_2 remains inside the expected wavenumber range.

Finally, we used SE to determine the broadband refractive index of the TiO_2:Ta_2O_5 coatings grown on Si, in their as-deposited form as well as after annealing at 500 °C. All measurements were performed in a wavelength range going from 620 to 2100 nm, except for pure Ta_2O_5 coating (0% TiO_2), where data are only available up to 1100 nm. SE data were modeled with a Cauchy dispersion relation, following the approach described in [13]. The resulting refractive index is reported in figure 6 as a function of %TiO_2. No data have been reported for the two samples with the highest TiO_2 content, upon annealing, as they undergo crystallization, and therefore their optical properties can no longer be described by the Cauchy dispersion relation. We refrain from presenting results from SE data analysis on partially crystallized samples as the presence of crystallites in those samples induces light scattering and depolarization. Given the increasing interest to shift the GWD laser wavelength from 1064 nm towards the near infrared [25], we report in table 2 the refractive index at some specific wavelengths, such as 1064, 1550, and 2000 nm. It is worth noting that the refractive index decreases with increasing wavelength in the considered spectral range (near-infrared). This is a common behavior of amorphous oxides, and in general of semiconductors with a large gap, where the main absorption band is in the UV region. Therefore, when developing a new coating design for GWDs, the effect of a lower refractive index to the coating thermal noise must be considered, since it will affect the overall coating thickness.

The optical properties of the pure TiO_2 and Ta_2O_5 coatings, shown here, are consistent with previous reports on similar coatings grown by IBS [26–28], even though a direct, quantitative comparison is never straightforward, due to the strong dependence of the coatings properties on the deposition parameters [29]. As expected, we observe a general increase of the refractive

Table 2. Tabulated refractive index n of as-deposited and annealed coatings at 1064 nm, 1550 nm, and 2000 nm.

	n @ 1064 nm		n @ 1550 nm		n @ 2000 nm	
% TiO_2	As-deposited	Ann.	As-deposited	Ann.	As-deposited	Ann.
0	2.062	2.046	—	2.033	—	2.029
25	2.105	2.083	2.088	2.068	2.081	2.063
50	2.147	2.125	2.130	2.107	2.124	2.100
75	2.219	2.172	2.196	2.153	2.186	2.146
80	2.236	—	2.212	—	2.203	—
100	2.270	—	2.246	—	2.237	—

index when increasing the Ti content, as pure TiO_2 coatings are optically denser than pure Ta_2O_5 ones. Annealing, on the other hand, results in coatings with lower refractive index, as observed in previous investigations for IBS-produced coatings [13, 27]. In fact, the thermal treatment produces relaxation of the highly compact IBS deposited coating, inducing both the lowering of the refractive index and the increase of the physical thickness [13, 26]. Unlike the mechanical loss measurements reported in [6], the optical properties are unaffected by the presence of pinhole defects, as their typical size (few tens of nm) is more than an order of magnitude smaller than the sampling light wavelength.

4. Conclusions

We performed a comprehensive study of TiO_2:Ta_2O_5 coatings for GWDs, by varying the TiO_2 content from 0% to 100%, and we provided valuable insights on how their morphological, structural, optical, and mechanical properties are affected by the cation ratio. First, our findings highlight the crucial role of substrate selection in determining the surface topography and roughness of the as-deposited coatings. These latter are strongly templated by the surface quality of the substrate, resulting, in the investigated cases, in a linear material arrangement, when deposited on SiO_2, and in an isotropic growth, when deposited on Si. As a result of substrates differences in surface quality and roughness, the deposited coatings show significantly different roughness values. This disparity underscores the importance of substrate quality for high-precision applications like GWD mirrors. Furthermore, our study reveals that at higher TiO_2 concentrations, pinhole-like defects appear in the coatings, impacting their surface quality. The density of these defects increases with increasing TiO_2 content, possibly reflecting the property of TiO_2 to be more susceptible to defect generation under ion bombardment. However, as proved by SE, the optical properties of the coatings seem unaffected by the presence of those defects. Furthermore, the study of the annealed coatings allowed to identify the amorphous-to-crystalline transition of both TiO_2 and Ta_2O_5 phases, as a function of % TiO_2. At low % TiO_2 ($<$50), the coatings remain amorphous upon the standard GWD mirror's annealing procedure (10 h at 500 °C). Higher annealing temperature induces the crystallization of the Ta_2O_5 phase first, and TiO_2 one later. At high % TiO_2 ($>$50), TiO_2 crystallizes below 500 °C, followed by Ta_2O_5 at much higher temperatures. Both XRD and RS confirm the existence of reciprocal strain effects between the TiO_2 and Ta_2O_5 phase, inside the coatings.

Our findings provide a valuable justification for the optical and mechanical results presented in [6, 13]. In [6], the authors demonstrate that: (i) the coating loss angle of 100% TiO_2 is few times higher than the one of mixed TiO_2:Ta_2O_5 (at low TiO_2 content); and (ii) the coating loss angle of 100% TiO_2 further increases upon annealing at 500 °C. We can now correlate the

result (i) to the presence of pinhole-like defects which contribute to increased internal friction, and thus mechanical losses; and the result (ii) to the structural TiO_2 transition, from amorphous to crystalline, which occurs below 500 °C (at 300 °C–350 °C). The coexistence of amorphous and crystalline phases, and related boundaries, spoils the optical and mechanical performance. On the other hand, we identify a range of TiO_2 content, nominally between ∼25% and 50%, but realistically between ∼15% and 38% (as measured by EBS), such that during annealing at 500 °C, the final coating exhibits optimal structural and morphological performance: the flatness of the coating is preserved, and no structural disorder, due to the formation of different phases, arises. Notably, the GWDs employ a 27% TiO_2 mixture strategically positioned in the middle of this interval. This result correlates with the behavior of the Urbach energy function measured in [13]. In summary, this study improves our understanding of TiO_2:Ta_2O_5 coatings for precision GWD mirrors, emphasizing the importance of substrate choice, and TiO_2 concentration, and deepening into the crystallization behavior.

Data availability statement

All data that support the findings of this study are included within the article (and any supplementary files).

Acknowledgments

The authors acknowledge Professor Pietro Campiglia, and Professor Carlo Crescenzi, from Pharmacy Department (DIFARMA) of University of Salerno for allowing the use of Raman microscope. The authors are also grateful to Professor Vincenzo Venditto and Dr Ivano Immediata, from the Chemistry and Biology Department (DCB) of University of Salerno for allowing the use of X-ray diffractometer. The authors acknowledge scientific discussions and contributions from all members of the VCR&D (Virgo Coating Research and Development) group of the Virgo collaboration and the Optics Working Group of the LIGO Scientific Collaboration. The authors acknowledge the financial support of INFN (Italian National Institute for Nuclear Physics) and EGO (European Gravitational Observatory), under the projects Virgo and ET-Italia.

ORCID iDs

Veronica Granata https://orcid.org/0000-0003-2246-6963
Michele Magnozzi https://orcid.org/0000-0003-4512-8430
Massimo Granata https://orcid.org/0000-0003-3275-1186
Francesco Chiadini https://orcid.org/0000-0002-9339-8622
Innocenzo M Pinto https://orcid.org/0000-0002-2679-4457
Fabrizio Bobba https://orcid.org/0000-0002-3472-642X

References

[1] Saulson P R 1990 Thermal noise in mechanical experiments *Phys. Rev.* D **42** 2437–45
[2] Levin Y 1998 Internal thermal noise in the LIGO test masses: a direct approach *Phys. Rev.* D **57** 659–63
[3] Callen H B and Greene R F 1952 On a theorem of irreversible thermodynamics *Phys. Rev.* **86** 702–10

[4] Crooks D R M *et al* 2002 Excess mechanical loss associated with dielectric mirror coatings on test masses in interferometric gravitational wave detectors *Class. Quantum Grav.* **19** 883–96
[5] Harry G M *et al* 2002 Thermal noise in interferometric gravitational wave detectors due to dielectric optical coatings *Class. Quantum Grav.* **19** 897–917
[6] Granata M *et al* 2020 Amorphous optical coatings of present gravitational-wave interferometers *Class. Quantum Grav.* **37** 095004
[7] Pierro V *et al* 2021 Ternary quarter wavelength coatings for gravitational wave detector mirrors: design optimization via exhaustive search *Phys. Rev. Res.* **3** 023172
[8] Durante O *et al* 2023 Investigation of crystallization in nanolayered TiO_2-based superlattices *Surf. Interfaces* **41** 103309
[9] Pinard L *et al* 2017 Mirrors used in the LIGO interferometers for first detection of gravitational waves *Appl. Opt.* **56** C11
[10] Harry G M *et al* 2006 Thermal noise from optical coatings in gravitational wave detectors *Appl. Opt.* **45** 1569
[11] Harry G M *et al* 2007 Titania-doped tantala/silica coatings for gravitational-wave detection *Class. Quantum Grav.* **24** 405–15
[12] Villar A E *et al* 2010 Measurement of thermal noise in multilayer coatings with optimized layer thickness *Phys. Rev.* D **81** 122001
[13] Amato A, Magnozzi M, Shcheblanov N, Lemaître A, Cagnoli G, Granata M, Michel C, Gemme G, Pinard L and Canepa M 2023 Enhancing titania-tantala amorphous materials as high-index layers in Bragg reflectors of gravitational-wave detectors *ACS Appl. Opt. Mater.* **1** 395–402
[14] Collaboration T V *et al* 2004 The VIRGO large mirrors: a challenge for low loss coatings *Class. Quantum Grav.* **21** S935–45
[15] Degallaix J *et al* 2019 Large and extremely low loss: the unique challenges of gravitational wave mirrors *J. Opt. Soc. Am.* A **36** C85
[16] Durante O *et al* 2021 Emergence and evolution of crystallization in TiO_2 thin films: a structural and morphological study *Nanomaterials* **11** 1409
[17] Hawash Z, Ono L K, Raga S R, Lee M V and Qi Y 2015 Air-exposure induced dopant redistribution and energy level shifts in spin-coated spiro-MeOTAD films *Chem. Mater.* **27** 562–9
[18] Takatsuji H and Arai T 2000 Pinholes in Al thin films: their effects on TFT characteristics and a Taguchi method analysis of their origins *Vacuum* **59** 606–13
[19] Tien C-L and Lee C-C 2003 Effects of ion energy on internal stress and optical properties of ion-beam sputtering Ta_2O_5 films *J. Mod. Opt.* **50** 2755–63
[20] Karmakar P, Liu G F and Yarmoff J A 2007 Sputtering-induced vacancy cluster formation on TiO_2 (110) *Phys. Rev.* B **76** 193410
[21] RRUFF database (available at: https://rruff.info/chem=Ti,O/display=default/R070582) (Accessed November 2023)
[22] Krishnaprasanth A and Seetha M 2018 Solvent free synthesis of Ta_2O_5 nanoparticles and their photocatalytic properties *AIP Adv.* **8** 055017
[23] Durante O *et al* 2023 Role of oxygen vacancies in the structural phase transformations of granular TiO_2 thin films *Surf. Interfaces* **37** 102698
[24] Allen N S, Mahdjoub N, Vishnyakov V, Kelly P J and Kriek R J 2018 The effect of crystalline phase (anatase, brookite and rutile) and size on the photocatalytic activity of calcined polymorphic titanium dioxide (TiO_2) *Polym. Degrad. Stab.* **150** 31–36
[25] ET Editorial Team 2020 Design report update 2020 for the Einstein telescope number: ET-0007B-20
[26] Magnozzi M *et al* 2018 Optical properties of amorphous SiO_2-TiO_2 multi-nanolayered coatings for 1064-nm mirror technology *Opt. Mater.* **75** 94–101
[27] Amato A, Terreni S, Granata M, Michel C, Pinard L, Gemme G, Canepa M and Cagnoli G 2019 Effect of heating treatment and mixture on optical properties of coating materials used in gravitational-wave detectors *J. Vac. Sci. Technol.* B **37** 062913
[28] Amato A *et al* 2019 Optical properties of high-quality oxide coating materials used in gravitational-wave advanced detectors *J. Phys. Mater.* **2** 035004
[29] Bundesmann C, Lautenschläger T, Spemann D, Finzel A, Thelander E, Mensing M and Frost F 2017 Systematic investigation of the properties of TiO_2 films grown by reactive ion beam sputter deposition *Appl. Surf. Sci.* **421** 331–40